World Academy of Science, Engineering and Technology
International Journal of Civil and Environmental Engineering
Vol:10, No:8, 2016

Numerical Modelling of Dry Stone Masonry Structures Based on Finite-Discrete Element Method

Ž. Nikolić, H. Smoljanović, N. Živaljić

***Abstract*—**This paper presents numerical model based on finite-discrete element method for analysis of the structural response of dry stone masonry structures under static and dynamic loads. More precisely, each discrete stone block is discretized by finite elements. Material non-linearity including fracture and fragmentation of discrete elements as well as cyclic behavior during dynamic load are considered through contact elements which are implemented within a finite element mesh. The application of the model was conducted on several examples of these structures. The performed analysis shows high accuracy of the numerical results in comparison with the experimental ones and demonstrates the potential of the finite-discrete element method for modelling of the response of dry stone masonry structures.

***Keywords*—**Finite-discrete element method, dry stone masonry structures, static load, dynamic load.

I. Introduction

A large part of cultural heritage all over the world are historical structures built as dry stone masonry. However, some of them which were originally built with mortar joints have experienced a significant loss of mortar during time and the behavior of these structures becomes similar to those made of dry stone masonry. Most of these structures have been damaged due to seismic activity [1]. With the aim of increasing their resistance, many of dry stone historical structures were further strengthened by steel clamps and bolts.

In order to evaluate the resistance of these structures and to be able to preserve the cultural heritage, it is necessary to develop a numerical model which could take into account all the effects occurring in dry stone masonry structures including the fragmentation of the blocks and non-linear behavior of steel clamps and bolts during dynamic loading.

The most commonly used numerical tool for the analysis of masonry structures is the finite element method where the material is regarded as a fictitious homogeneous orthotropic continuum [2]-[4]. The other attractive tools for modelling of dry stone masonry structures are based on a discrete element method [5]-[10]. The common idea in different applications of the discrete element method to masonry structures is idealization of the material as a discontinuum where joints are modelled as contact surfaces between different blocks. This approach is suitable for modelling different types of non-linear behavior including large displacements and rotation with complete detachment of blocks.

In recent times, an increasing number of models attempted to combine the advantages of finite and discrete element methods [11]-[14]. One of these methods is finite-discrete element method (FEM/DEM) [15] which was successfully applied in 2D analysis of dry stone masonry structures [16] and dry stone masonry structures strengthened with clamps and bolts [17]. The model based on this method is capable of predicting the collapse mechanism and collapse load of dry stone masonry structures under static and seismic loads. Since the stone structures are mainly three-dimensional massive, modeling of those structures requires a 3D model. Therefore, the previously developed 2D finite discrete numerical model for stone masonry structures strengthened with clamps and bolts is extended for analysis of different failure mechanisms occurred in 3D stone masonry structures. The model can be useful in making the right decisions during the restoration of dry stone masonry structures, especially those classified as cultural heritage.

II. Types of Steel Clamps and Bolts

Historical dry stone masonry structures are commonly strengthened with steel clamps embedded on the lateral surface of the structure (Fig. 1 (a)) or on the top side of stone blocks (Fig. 1 (b)), as well as with steel bolts (Fig. 1 (c)).

(a) (b) (c)

Fig. 1 Steel clamps and bolts: (a) steel clamp embedded on the lateral face of the structure; (b) steel clamp embedded on the top side of stone blocks; (c) steel bolts [17]

Clamps and bolts are embedded into the previously made holes in stone blocks that are subsequently backfilled with some infill material like plumb.

Clamps are most commonly used in strengthening of dry stone walls and dry stone arches by tension bearing capacity while steel bolts are used for connecting the capitals and columns or capitals and upper beams (Fig. 1 (c)) and they dominantly have shear bearing capacity.

Due to the presence of many parameters which effect on

Ž. Nikolić and N. Živaljić are with the University of Split, Faculty of Civil Engineering, Architecture and Geodesy, 21000 Split, HR-Croatia (phone: +385-21-303332; fax: +385-21-465117; e-mail: zeljana.nikolic@gradst.hr, nikolina.zivaljic@gradst.hr).

H. Smoljanović, is with the University of Split, Faculty of Civil Engineering, Architecture and Geodesy, 21000 Split, HR-Croatia (phone: +385-21-303380; fax: +385-21-465117; e-mail: hrvoje.smoljanovic@gradst.hr).

behavior of clamps and bolts in dry stone masonry structures, such as the elastic properties of stone and steel, the width and depth of the hole into which the clamps and bolts are embedded, elastic properties of infill material, geometry of clamps and bolts etc., it is very difficult to develop numerical model which can take into account all types of failure mechanisms and especially the influence of local interaction between the bolt or clamp on one side and masonry block on another. This paper presents numerical model for steel clamps and bolts which are embedded into 3D finite-discrete model for stone masonry structures. The model is an extension of previously developed 2D model [16].

Schematic presentations of steel clamps and steel bolts modelled in this paper are shown in Fig. 2.

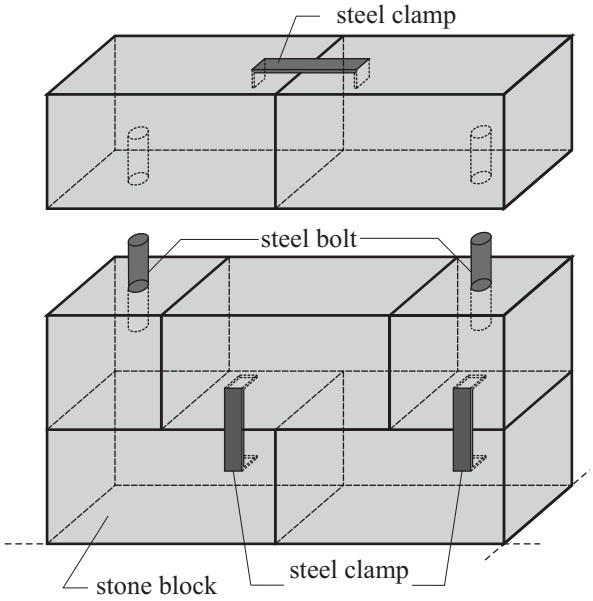

Fig. 2 Steel clamps and bolts

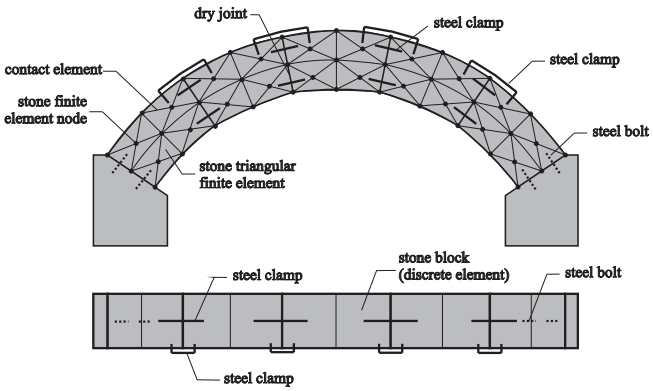

Fig. 3 Discretization of dry stone structure with steel clamps and bolts

III. Discretization of a Dry Stone Structure with Steel Clamps and Bolts

Each stone block is modelled as a discrete element which is discretized by constant 2D triangular or 3D tetrahedron finite elements. Contact interaction between stone blocks is considered through the contact interaction algorithm based on the principle of potential contact forces [18], [19] which include the Coulomb-type law for friction [20]. Material non-linearity, fracture and fragmentation are considered through the contact elements which are placed within the finite element mesh of each block.

The steel clamps and steel bolts were modelled with one-dimensional elements which can be placed in arbitrary positions inside the stone finite elements.

Discretization of dry stone masonry structure with embedded steel clamps and bolts is shown in Fig. 3.

IV. Non-Linear Material Model of Stone Blocks

The material model of stone blocks is based on crack initiation and crack propagation in tension and shear [15]. The area under the stress-strain curve consists of two parts (Fig. 4), part for modelling of the stone behavior up to the crack opening and part which represents strain softening after the tensile strength is exceeded. The assumption of the discrete crack model is that the cracks coincide with the finite element edges. The total number of nodes for each of the finite element meshes is doubled and the continuity between elements is realized through the penalty method [18]. Separation of the edges induces a bonding stress, which is a function of the separation size δ.

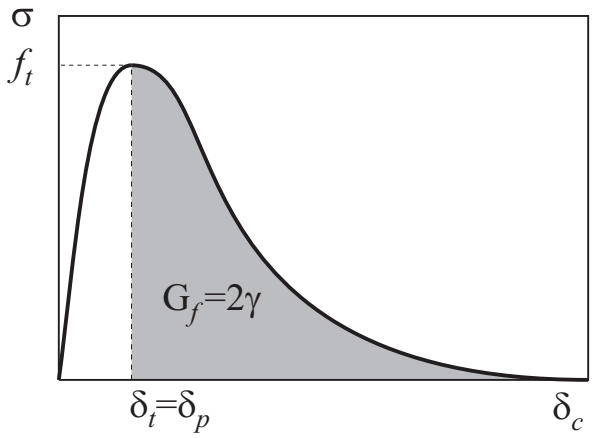

Fig. 4 Strain softening stress-strain and stress-displacement curves

The area under the stress-displacement curve represents the fracture energy $G_f=2\gamma$, where γ is the surface energy, i.e. the energy needed to extend the crack surface by a unit area. The edges of two adjacent elements are held together by normal and shear springs before the tensile strength is reached (Fig. 5). Procedure of the separation of the elements and complete relationship for the normal and shear bonding stress are given in [15].

V. Numerical Model of Steel Clamps

A. Steel material model

The stress-strain relationship for a monotonically increasing loading in steel is shown in Fig. 6 (a). The hysteresis behavior

of steel is modelled by Kato's stress-strain model [21] which is shown in Fig. 6 (b).

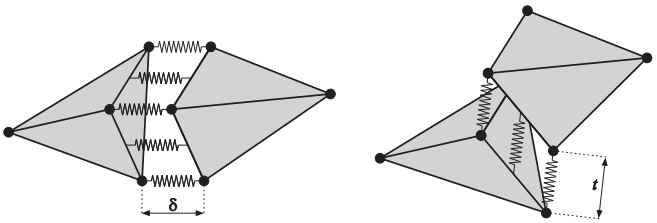

Fig. 5 Normal and shear springs between the finite elements

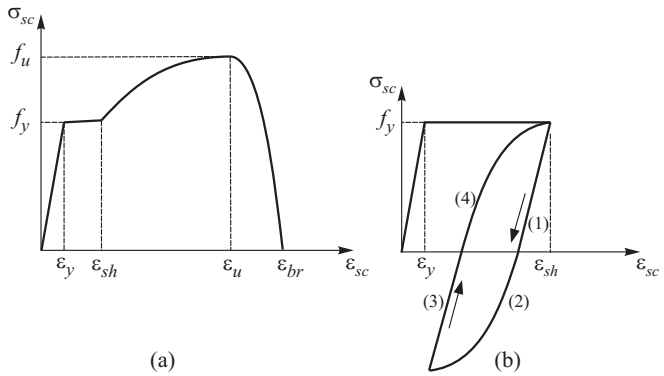

Fig. 6 Stress-strain model of steel: (a) monotonic loading; (b) cyclic loading (Kato)

From the given strain, stress is calculated by the following expressions:

1. during unloading (Fig. 6 (b), curve (1))

$$\sigma_{sc} = f_y - E_s(\varepsilon_{sh} - \varepsilon_{sc}) \tag{1}$$

where E_s is Young's modulus of steel.

2. during negative loading (Fig. 6 (b), curve (2))

$$\sigma_{sc} = -f_y\left[\frac{a - \{a(a-1)\}}{-(E_B/f_y)(\varepsilon_{sc} - \varepsilon_{sh} + \varepsilon_y) + a - 1}\right] \tag{2}$$

where $E_B = -(E_s/6)\log 10(\varepsilon_{sh} - \varepsilon_y)$, $a = E_s/(E_s - E_B)$;

3. during reloading-unloading (Fig. 6 (b), curve (3))

$$\sigma_{sc} = \sigma_{pm} + E_s(\varepsilon_{sc} - \varepsilon_{pm}) \tag{3}$$

where σ_{pm} is the minimum value of σ_{sc} in its loading history;

4. during reloading (Fig. 6 (b), curve (4))

$$\sigma_{sc} = f_y + \sigma_{pm} - f_y\left[\frac{a - \{a(a-1)\}}{-(E_B/f_y)(\varepsilon_{sc} - \varepsilon_{sh} + \varepsilon_y) + a - 1}\right] \tag{4}$$

B. Steel Clamps

The steel clamp was defined by its first point P_0, the end point P_1 and the anchorage length l_k (Fig. 7). The intersection between the blocks edges and line segment $\overline{P_0P_1}$ gives the referents points R_0 and R_1. The strain of a steel clamp in arbitrary time step can be obtained from the coordinates of these points in current configuration.

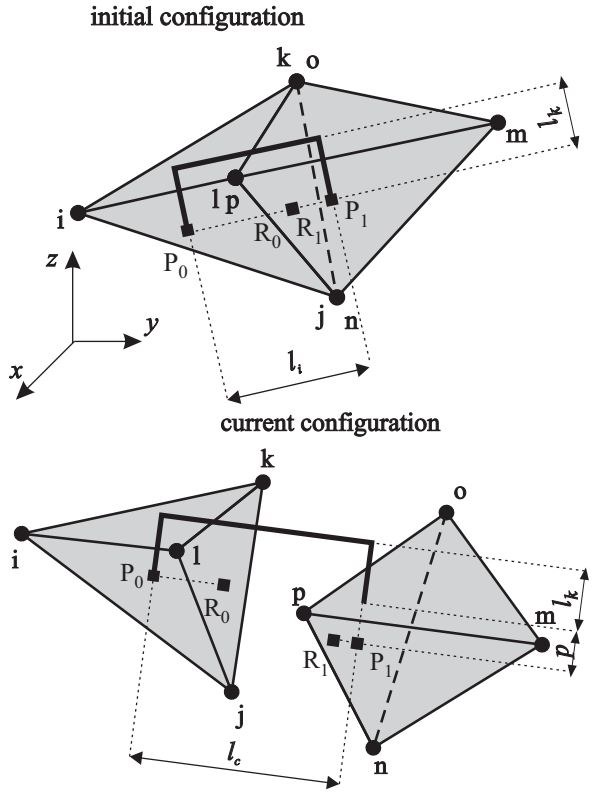

Fig. 7 Steel clamp in initial and current configuration.

Coordinates of point P_0 in current configuration are obtained according to

$$\begin{aligned} x_{0c} &= Ax_{ic} + Bx_{jc} + Cx_{kc} + Dx_{lc} \\ y_{0c} &= Ay_{ic} + By_{jc} + Cy_{kc} + Dy_{lc} \\ z_{0c} &= Az_{ic} + Bz_{jc} + Cz_{kc} + Dz_{lc} \end{aligned} \tag{5}$$

where x_c, y_c and z_c are coordinates of particular node in current configuration. Unknown coefficients A, B, C and D can be obtained from

$$A = \frac{V_i}{V};\ B = \frac{V_j}{V};\ C = \frac{V_k}{V};\ D = \frac{V_l}{V} \tag{6}$$

where V is the volume of the corresponding tetrahedron while V_i, V_j, V_k, and V_l are volume of tetrahedrons defined by points $0jkl$, $0ikl$, $0ijl$ and $0ijk$ respectively. Coordinates of point P_1, R_0 and R_1 in current configuration can be obtained in similar way.

Strain of steel clamp is given by

$$\varepsilon_{sc} = \frac{l_c - l_i}{l_i} \tag{7}$$

where l_c and l_i are lengths of a steel clamp in current and initial configurations respectively. From obtained strain, it is possible to calculate stress σ_{sc} of the steel clamp from the steel material model.

The influence of tangential separation p is approximately taken into account through a reduction of stress σ'_{sc} given by

$$\sigma'_{sc} = z\sigma_{sc} \tag{8}$$

where z is the scaling function. The scaling function is equal to one when there is no shear separation, while it is equal to zero when the shear separation is equal to l_k. For shear separation $0<p<l_k$ the scaling function depends on the elastic properties of stone and a steel clamp, the width of the hole in which the steel clamp is embedded, the elastic properties of the infill material, the cross section area of the clamp, etc. In this numerical model the scaling function is assumed as [22]

$$z = 1.0 - \frac{e^{-\alpha} D}{1.0 + \left(e^{-\alpha} - 1.0\right) D} \tag{9}$$

where variable $D=D(p)$ is determined according to:

$$D(p) = \begin{cases} 0.0 \quad \text{for} \quad p = 0.0; \\ 1.0 \quad \text{for} \quad p \geq l_k; \\ p / l_k \quad \text{other} \end{cases} \tag{10}$$

The shape of function z for different values of shape parameter α is shown Fig. 8.

In absence of experimental results, the shape parameter $\alpha = \alpha_c$ for steel clamps can be initially set to zero which leads to a linearly decreasing function. If experimental results exist, parameter α_c can be chosen to best fit experimental data.

The force in a steel clamp (Fig. 9 (a)) is given by

$$\left|\mathbf{f}_{0sc}\right| = \left|\mathbf{f}_{1sc}\right| = A_{sc}\sigma'_{sc} \tag{11}$$

where A_{sc} is the cross-sectional area of clamp.

Forces $\mathbf{f}_{0sc}$ and $\mathbf{f}_{1sc}$ acting in points P_0 and P_1 are distributed into the nodes of the parent stone triangular finite element in the form of equivalent nodal forces (Fig. 9 (b)).

A. Behavior of Clamps under Monotonic Loading

The behavior of clamps under monotonic loading was performed on two rigid tetrahedrons connected with a steel clamp (Fig. 10). The material characteristics of the steel clamp are shown in Table I.

The monotonically increasing load was performed in terms of constant velocity v_x and v_y in point B. Velocity v_x was equal v_x =0.2 m/s while velocity v_y was varied with values of 0.0 m/s, 0.2 m/s, 0.3 m/s and 0.4 m/s.

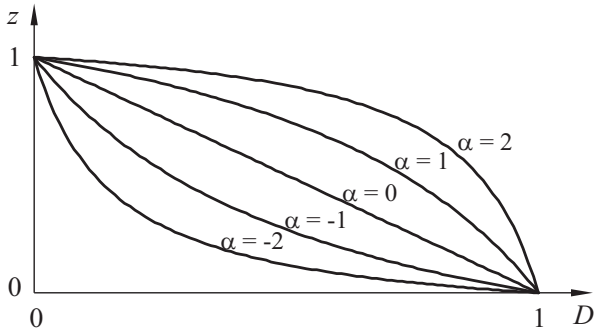

Fig. 8 Reduction factor for different values of shape parameter α

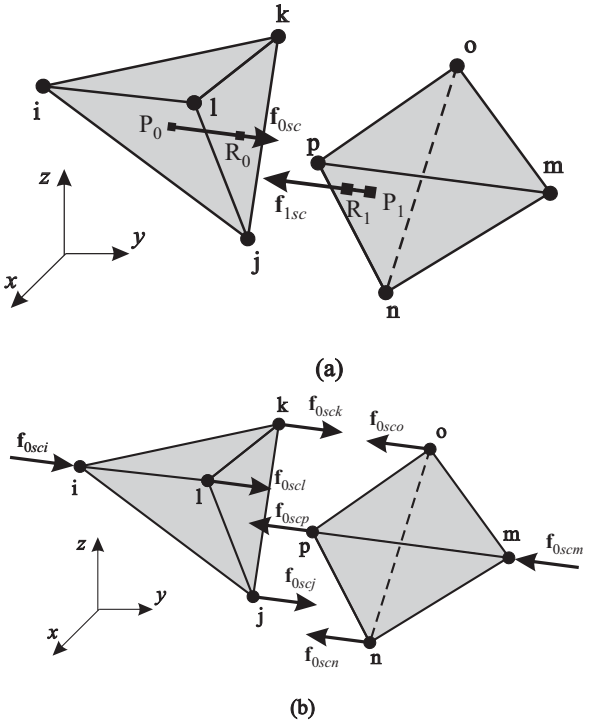

Fig. 9 Steel clamp: (a) force in steel clamp; (b) equivalent nodal forces

TABLE I
MATERIAL CHARACTERISTICS OF STEEL

Symbol	Quantity	
E_s	Modulus of elasticity	183 000 MPa
fy	Yield stress	446 MPa
fu	Ultimate stress	640 MPa
As	Cross section area	0.05 m^2
ε_{sh}	Strain (end of yield)	0.005
ε_u	Ultimate strain	0.100
ε_{br}	Break strain	0.120

The stress-strain relation in a steel clamp for all cases of loading is shown in Fig. 10. It can be seen that, for velocities v_y different from zero, the reduction in stress occurs due to the extracting of the steel clamp from the stone block. Extracting of the steel clamp from the block increases with the increase of the velocity v_y, this leads to the additional reduction of the stress in the steel clamp.

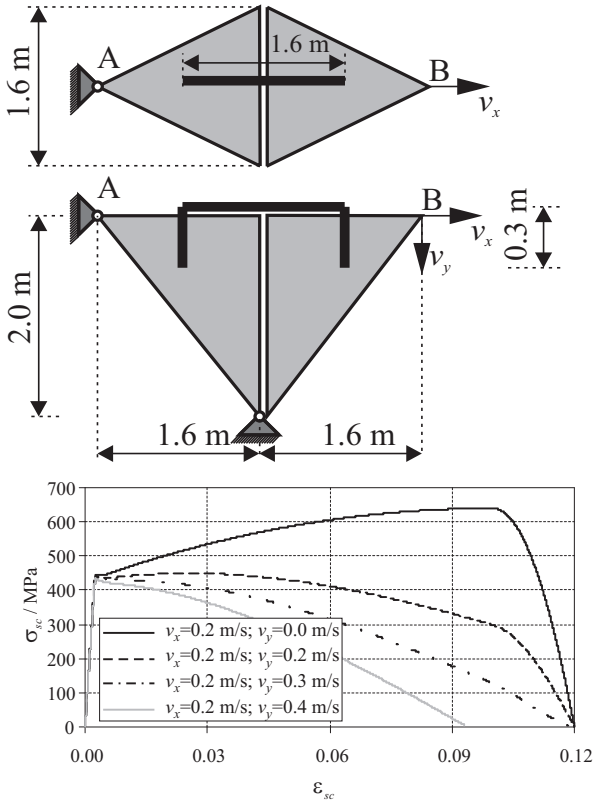

Fig. 10 Stress-strain relation in steel clamps for different cases of loading

VI. Numerical Model of Steel Bolts

A. Geometry and Material Model of the Bolts

The steel bolt was defined by its first point P_0 and the end point P_1. The intersection between the blocks edges and line segment gives the referents points R_0 and R_1 (Fig. 11). The coordinates of points P_0, P_1, R_0 and R_1 in current configuration are obtained in a similar way as it was shown in steel clamps model.

Tangential separation s induces shear stress τ_{sb} in the steel bolt and at separation $s=s_{pb}$ the shear stress reaches its maximum f_{su} (Fig. 12 (a)). With increasing tangential separation $s>s_{pb}$ shear stress decreases and at separation $s>s_{tb}$ it drops to zero and the bolt is assumed to be broken.

Values of f_{su}, s_{pb}, s_{tb} and shape of functions, which define the relation between shear separation and shear stress, depends on elastic properties of stone and a steel bolt, the width of the hole in which the steel bolt is embedded, the elastic properties of the infill material, the cross section area of the bolt, etc., and need to be determined experimentally for each particular case.

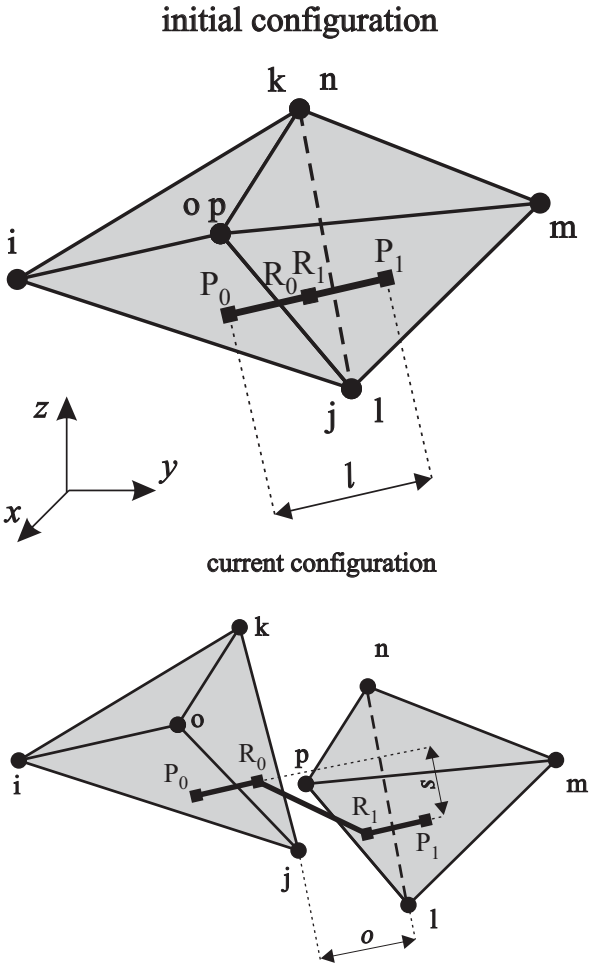

Fig. 11 Steel bolt in initial and current configuration

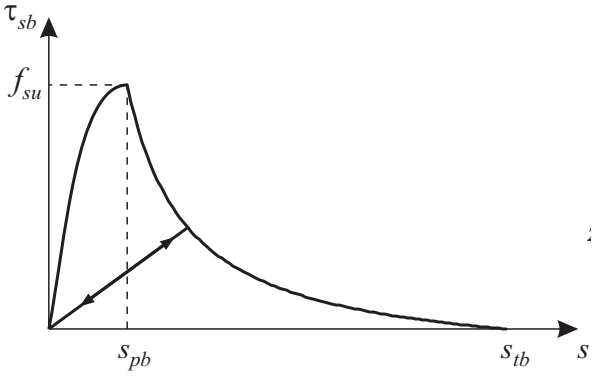

(a)

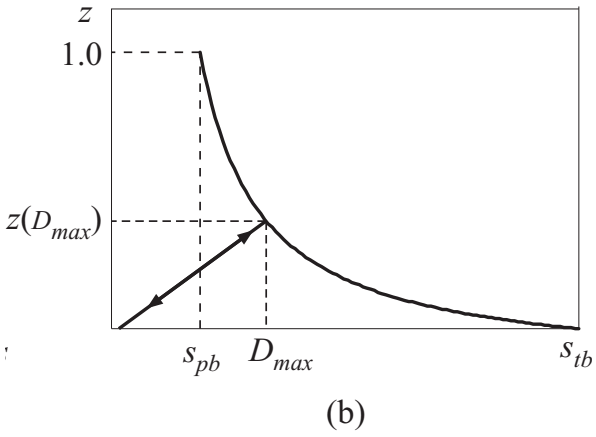

Fig. 12 Material model in the steel bolt: (a) shear stresses versus shear separation, (b) cyclic behavior

The maximum value of shear stress f_{su} in steel bolt is limited with shear strength of bolt material f_{sb} which can be written as

$$f_{su} \le f_{sb} \tag{12}$$

and with shear stress in bolt which cause local crushing of stone around the bolt. The shear strength of steel f_{sb} can be determined from the tensile strength f_u by applying the Von Mises yield criterion which leads to

$$f_{sb} = \sqrt{1/3} f_u \tag{13}$$

Taking into account that the local compressive strength of stone is 3.3 times higher than the global compressive strength f_c [23] and assuming that in the case of local crushing of stone around the bolt the compressive stress in bolt linearly decreases to a depth of three diameters of bolt, it can be written as

$$f_{su} \frac{d^2 \pi}{4} \le 3d^2 (3.3 f_c)/2 \tag{14}$$

which leads to

$$f_{su} \le 6.3 f_c \tag{15}$$

where d is diameter of bolt.

In actual implementation for separation $0 \le |s| < s_{pb}$ shear stress is given by

$$\tau_{sb} = \left(2\frac{s}{s_{pb}} - \left(\frac{s}{s_{pb}} \right)^2 \right) f_{su} \tag{16}$$

where value of s_{pb} is treated as input parameter. For separation $s_{pb} \le |s| < s_{tb}$ shear stress is assumed as

$$\tau_{sb} = z f_{su} \tag{17}$$

where z is the scaling function defined with (17) where

$$D = D(s) = \begin{cases} 0.0 & \text{for} \quad |s| < s_{pb}; \\ 1.0 & \text{for} \quad s \ge s_{tb}; \\ (|s| - s_{pb}) / (s_{tb} - s_{pb}) & \text{other} \end{cases} \tag{18}$$

The value of the shape parameter $\alpha = \alpha_{bs}$ needs to be chosen to best fit experimental data. In the absence of experimental data, it can be set to initial value $\alpha_{bs}=0$. However, collapse of the stone masonry structures usually occurs due to the loss of the global stability and this parameter has no influence on the global structural behaviour. If the collapse of the structure caused by the breaking of the bolts, parameter α_{bs} has only influence on the shape of the load-displacement curve in softening phase, but not to the value of collapse load.

The complete relationship for the shear stress as the function of shear separation can be written as

$$\tau_{sb} = \begin{cases} \left(2\frac{|s|}{s_{pb}} - \left(\frac{|s|}{s_{pb}} \right)^2 \right) f_{su} z & \text{for} \quad |s| \le s_{pb}; \\ z f_{su} & \text{for} \quad |s| \le s_{pb} \end{cases} \tag{19}$$

The influence of normal separation o is approximately taken into account through a reduction of stress τ'_{sb} given by

$$\tau'_{sb} = z \tau_{sb} \tag{20}$$

where z is the scaling function. The scaling function is equal to one when there is no normal separation while it is equal to zero when the normal separation is equal to $l/2$ where l is the steel bolt length. For normal separation $0 < o < l/2$ the scaling function depends of elastic properties of stone and a steel bolt, the width of the hole in which the steel bolt is embedded, the elastic properties of the infill material, the cross section area of the bolt, etc. In this numerical model the scaling function is assumed according to (17) where the variable $D = D(o)$ is determined according to

$$D = D(o) = 2o / l \tag{21}$$

Cyclic behaviour of bolt (Fig. 13) is assumed as

$$z = z(D_{max}) \frac{D(s_{tb} - s_{pb}) + s_{pb}}{D_{max}(s_{tb} - s_{pb}) + s_{pb}} \tag{22}$$

where D_{max} is the maximum value of $D(s)$ in its loading history.

Shear force in the steel bolt (Fig. 13 (a)) is given by

$$\left|\mathbf{f}_{0sb}\right| = \left|\mathbf{f}_{1sb}\right| = A_{sb}\tau_{sb} \tag{23}$$

where A_{sb} is cross-section area of the bolt.

Forces $\mathbf{f}_{0sb}$ and $\mathbf{f}_{1sb}$ which are assumed to act in the centre of the bolt anchored in the stone block, are distributed into the nodes of the parent stone triangular finite element in the form of equivalent nodal forces (Fig. 13 (b)).

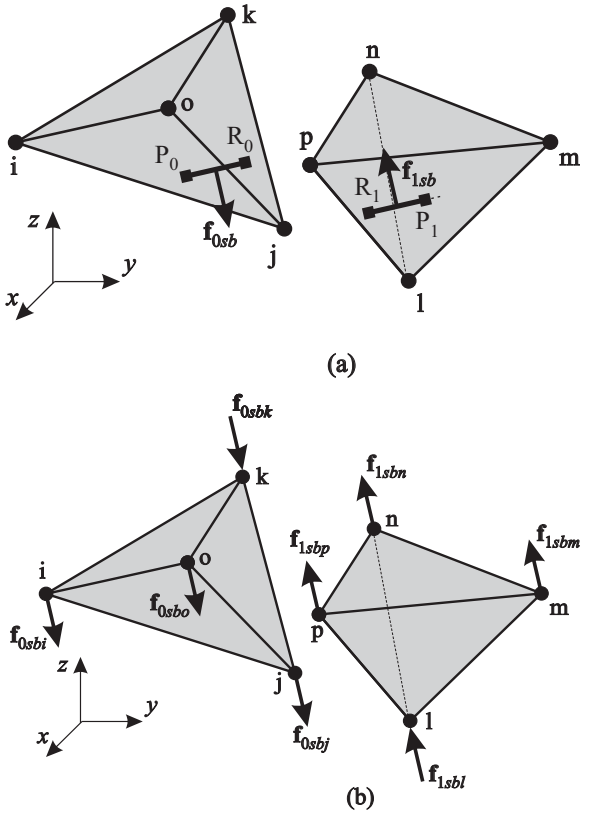

Fig. 13 Steel bolt: (a) force in steel bolt; (b) equivalent nodal forces

B. Behavior of Bolts under Monotonic Loading

The behaviour of the model of bolts under monotonic loading was performed on two rigid tetrahedrons connected with steel bolt (Fig. 14). The parameters applied in the numerical analysis are shown in Table II.

TABLE II
NUMERICAL PARAMETER OF STEEL BOLT

Symbol	Quantity	
D	Diameter	50 mm
f_{tb}	Tangential strength	369.5 MPa
s_{pb}	Ultimate tangential separation	0.05 mm
s_{tb}	Break tangential separation	3.00 mm

The monotonically increasing load was performed in terms of constant velocity v=0.2 m/s in point B. Initial normal displacement o in numerical analysis was varied with values of 0.0 m, 0.05 m and 0.075 m.

Shear stress-shear separation relations in steel bolts for different initial normal displacement are shown in Fig. 14. It can be seen that increasing the initial normal displacement, the reduction in shear stresses also increases.

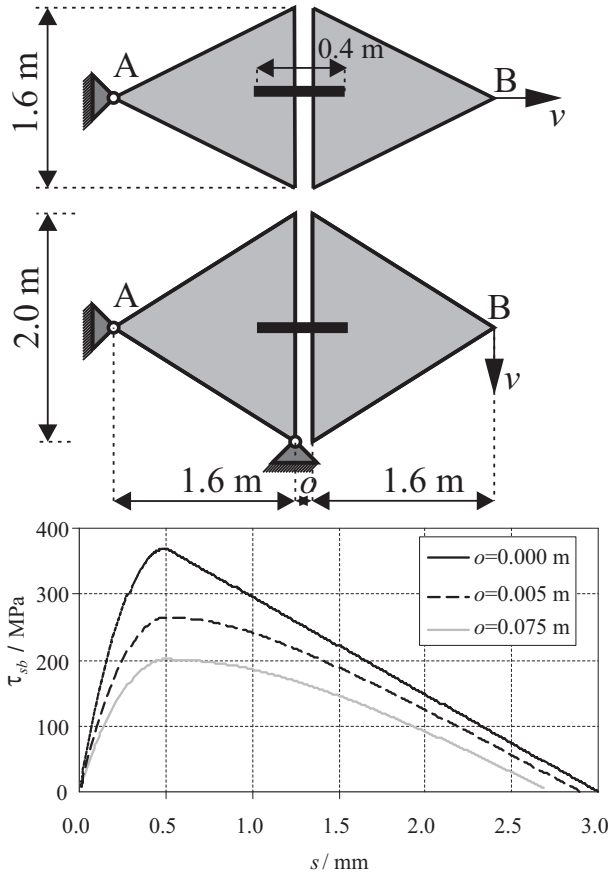

Fig. 14 Shear stress - shear separation relations in steel bolt for different initial normal displacement

VII. THE VERIFICATION OF THE MODEL

An example of a dry stone masonry wall under monotonic and cyclic loads with the known experimental and numerical results [24], [25] was used for verification of the model under monotonic and cyclic load conditions. The geometry and finite element mesh are shown in Fig. 15. The numerical analysis was performed for vertical pre-compression load 250 kN which corresponds to the pre-compression stress of 1.25 MPa. After applying the vertical load, the horizontal load in terms of controlled horizontal displacement was applied at the top of the steel beam (Fig. 15).

The wall consisted of the sawn stone units with the dimensions of 200 mm (length) × 150 mm (height) × 200 mm (width). Contact elements which present potential cracks in stone units are implemented between the finite element mesh. Mechanical characteristics of the contact elements are: Young's Modulus E=20200 MPa, tensile strength f_t=2.8 MPa, compressive strength f_c=69.2 MPa, fracture energy G_f^I =186 N/m and sliding friction μ =0,65. The cyclic loading history is shown in Fig. 16.

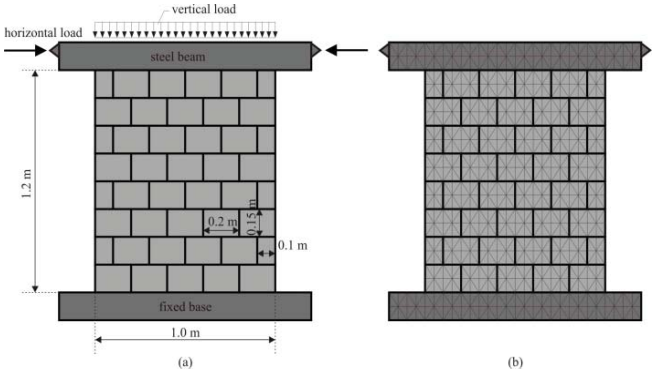

Fig. 15 Dry stone masonry wall: (a) geometry; (b) finite element mesh

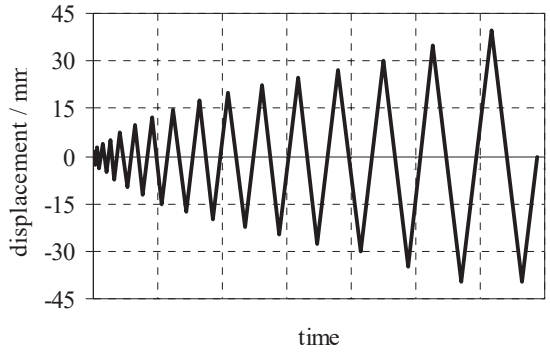

Fig. 16 Loading history

The results of the model were compared with the experimental [24] and numerical results obtained by Senthivel and Lourenço [25] for a monotonically increasing load (Fig. 17). The force-displacement curve under monotonic load obtained by the FEM/DEM method assuming potential cracks in blocks are very close to the experimental curves and numerical result obtained by the analysis where potential cracks in the units were not considered [25].

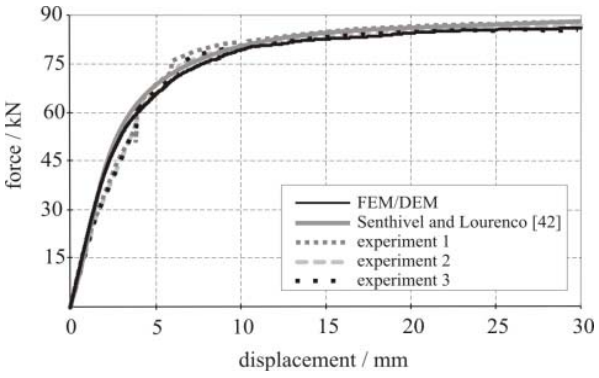

Fig. 17 Force-displacement diagram under monotonic loading

The results of the model were also compared with the experimental result for cyclic load (Fig. 18).

Fig. 18 shows that the force-displacement curve under cyclic loads obtained numerically is very close to the experimental curve. The failure pattern after reaching ultimate load obtained from experiment and numerical analysis (Fig. 19) is also very similar.

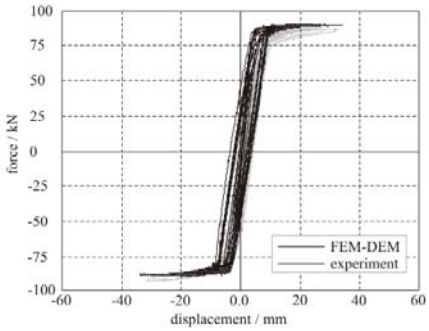

Fig. 18 Force-displacement diagram under cyclic loading

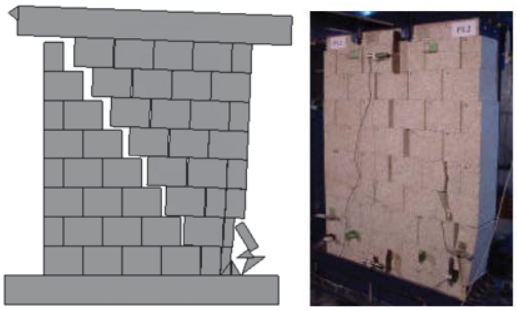

Fig. 19 Failure pattern of dry masonry wall (numerical and experimental)

VIII. Conclusion

This paper presents numerical model for analysis and prediction of the collapse of dry stone masonry structures strengthened with steel clamps and bolts which is based on the finite-discrete element method. The developed model can be used for the estimation of the seismic resistance of historical dry stone masonry structures reinforced with steel clamps and steel bolts, which is very important for the structures classified as cultural heritage. The model can also help to make the right decisions regarding the restoration of dry stone masonry structures which have experienced deterioration over time.

Acknowledgment

This work has been fully supported by Croatian Science Foundation under the project *Development of numerical models for reinforced-concrete and stone masonry structures under seismic loading* based on discrete cracks (IP-2014-09-2319).

References

[1] F. Parisi, N. Augenti, "Earthquake damages to cultural heritage constructions and simplified assessment of artworks," *Engineering Failure Analyses*, vol. 34, pp. 735-760, 2013.

[2] P.B. Lourenço, J.G. Rots and J. Blaauwendraad, "Continuum model for masonry: parameter estimation and validation," *Journal of Structural Engineering ASCE*, vol. 1(6), pp. 642-652, 1998.

[3] L. Berto, A. Saetta, R. Scotta and R. Vitaliani, "An orthotropic damage model for masonry structures," *International Journal of Numerical Methods in Engineering*, vol. 55, pp.127-157, 2002.

[4] S. Casolo, "Macroscopic modelling of structured materials: Relationship between orthotropic Cosserat continuum and rigid elements,"

International Journal of Solids and Structures, vol. 43(3-4), pp. 475-496, 2006.

[5] P.A. Cundall, "A computer model for simulating progressive large scale movements in blocky rock systems (Published Conference Proceedings style)," in *Proc. of the Symposium on Rock Fracture (ISRM)*, Nancy, France, 1971, pp. 1-8.

[6] P.A. Cundall, R.D. Hart, "Numerical modelling of discontinua," *Engineering Computations*, vol. 9, pp. 101-113, 1992.

[7] C. Baggio, P. Trovalusci, "Stone assemblies under in-plane actions-comparison between nonlinear discrete approaches," *Computer Methods in Structural Masonry*, vol. 3, pp. 184-193, 1995.

[8] C. Baggio, P. Trovalusci, "Collapse behaviour of three-dimensional brick-block systems using non-linear programming," *Structural Engineering and Mechanics*, vol. 10, pp. 181-195, 2000.

[9] A. Nappi, F. Tin-Loi, "A numerical model for masonry implemented in the framework of a discrete formulation," *Structural Engineering and Mechanics*, vol. 11(2), pp. 171-184, 2001.

[10] M. Gilbert, C. Casapulla, H. M. Ahmed, "Limit analysis of masonry block structures with non-associative frictional joints using linear programming," *Computers & Structures*, vol. 84(13), pp. 873-887, 2006.

[11] P.A. Cundall, "Formulation of a three-dimensional distinct element model – Part I: A scheme to detect and represent contacts in a system composed of many polyhedral blocks," *International Journal of Rock Mechanics and Mining Sciences*, vol. 25 (3), pp. 107-116, 1988.

[12] R. D. Hart, P. A. Cundall and V. Lemos, "Formulation of a three-dimensional distinct element model–Part II: Mechanical calculations," *International Journal of Rock Mechanics and Mining Sciences*, vol. 25(3), pp. 117-125, 1988.

[13] N. Petrinic, *Aspects of discrete element modelling involving facet-to-facet contact detection and interaction*. Ph.D. dissertation, UK: University of Wales, 1996.

[14] G. H. Shi, R. E. Goodman, "Discontinuous deformation analysis- A new method for computing stress, strain and sliding of block systems," in *Key Questions in Rock Mechanics*, Rotterdam Balkema, 1988, pp. 381-393.

[15] A. Munjiza, *The combined finite-discrete element method*. 1st ed. UK: John Wiley & Sons, 2004.

[16] H. Smoljanović, N. Živaljić and Ž. Nikolić, "A combined finite-discrete element analysis of dry stone masonry structures," *Engineering Structures*, vol. 52, pp. 89-100, 2013.

[17] H. Smoljanović, Ž. Nikolić and N. Živaljić, "A finite-discrete element model for dry stone masonry structures strengthened with steel clamps and bolts", *Engineering Structures*, vol. 90, pp. 117-129, 2015.

[18] A. Munjiza, K. R. F. Andrews and J.K. White, "Penalty function method for combined finite-discrete element system comprising large number of separate bodies", *International Journal for Numerical Methods in Engineering*, vol. 49, pp. 1377-1396, 2000.

[19] A. Munjiza, K. R. F. Andrews and J.K. White, "NBS contact detection algorithm for bodies of similar size", *International Journal for Numerical Methods in Engineering*, vol. 43, pp. 131-149, 1998.

[20] J. Xiang, A. Munjiza, J.P. Latham and R. Guises, "On the validation of DEM and FEM/DEM models in 2D and 3D", *Engineering Computations*, vol. 26, pp. 673-687, 2000.

[21] B. Kato, "*Mechanical properties of steel under load cycles idealizing seismic action",* Structural concrete under seismic actions, AICAP-CEB symposium, vol. 132, pp. 7-27, 1979.

[22] I. Carol, P. Prat and C.M. López, "Normal/Shear Cracking Model: Application to Discrete Crack Analysis", *Journal of Engineering Mechanics*, vol. 123 (8), pp. 765–773, 1997.

[23] Comite European de Normalization (CEN), *Eurocode 2: Design of concrete structures*, EN 1992-1-1, Brussels, 2004.

[24] G. Vasconcelos, *Experimental investigations on the mechanics of stone masonry: Characterization of granites and behaviour of ancient masonry shear walls,* Ph.D. dissertation. GUIMARÃES, Portugal: University of Minho, 2005.

[25] R. Senthivel and P.B. Lourenço, "Finite element modelling of deformation characteristics of historical stone masonry shear walls*", Engineering Structures*, vol. 31, pp. 1930-1943, 2009.